Geophysical Research Letters®

RESEARCH LETTER
10.1029/2021GL094592

Key Points:

- Interannual variability in sea level along the west Australian coast can be predicted up to 13 months in advance using a simple ocean model
- To illustrate, the model is run in hindcast mode forced remotely by Pacific surface winds related to El Niño Southern Oscillation
- Model hindcasts generally outperform persistence forecasts in terms of anomaly correlation and root-mean-squared differences

Supporting Information:

Supporting Information may be found in the online version of this article.

Correspondence to:

M. Nagura,
nagura@jamstec.go.jp

Citation:

Nagura, M., & McPhaden, M. J. (2021). Predicting interannual variability in sea surface height along the west coast of Australia using a simple ocean model. *Geophysical Research Letters*, *48*, e2021GL094592. https://doi.org/10.1029/2021GL094592

Received 29 MAY 2021
Accepted 30 AUG 2021

Predicting Interannual Variability in Sea Surface Height Along the West Coast of Australia Using a Simple Ocean Model

Motoki Nagura[1] and Michael J. McPhaden[2]

[1]Japan Agency for Marine-Earth Science and Technology, Yokosuka, Japan, [2]National Oceanic and Atmospheric Administration/Pacific Marine Environmental Laboratory, Seattle, WA, USA

Abstract Sea surface height (SSH) along the west coast of Australia is key to local climate and is strongly forced by remote surface wind variability related to El Niño Southern Oscillation (ENSO) in the tropical Pacific Ocean. This study provides a method to predict interannual variability in SSH along the west coast of Australia using a simple 1.5-layer dynamical ocean model forced by a statistical atmospheric model for ENSO-related winds. The model has realistic coastlines and is driven by reanalysis surface winds regressed onto an ENSO index. The model when run in hindcast mode to predict past variability can simulate tide gauge observations at Fremantle along the west coast of Australia up to 13 months in advance, which outperforms persistence. We conclude that this methodology can be useful as a baseline for gauging the performance of more sophisticated forecast models for predicting SSH variations along the west coast of Australia.

Plain Language Summary Sea surface height (SSH) along the west coast of Australia is key to regional climate and is strongly forced by remote surface wind variability related to El Niño Southern Oscillation (ENSO) in the tropical Pacific Ocean. Previous studies predicted interannual variability in SSH in this region using sophisticated ocean-atmosphere coupled general circulation models, but their ocean models had coarse horizontal resolution, required to reduce computational burden. This study provides a much simpler method to predict SSH variability along the west coast of Australia using a simple ocean dynamical model with realistic coastlines forced by ENSO-related atmospheric winds. Our model, run in hindcast mode to predict past SSH variability, is able to simulate SSH anomalies along the west coast of Australia up to 13 months in advance. A true forecast system to predict future variations would also require prediction of ENSO. However, this methodology can be useful as a baseline for gauging the performance of more sophisticated model forecast systems.

1. Introduction

Sea surface height (SSH) along the west coast of Australia shows marked interannual and decadal variability (Feng et al., 2010, 2011) and is key to understanding climate variability in the tropical and southeastern Indian Ocean. Anomalously elevated (or depressed) SSH along the west coast of Australia often accompanies warm (cool) surface water, which is known as a Ningaloo Niño (Niña) event and can cause coral bleaching, fish kills and anomalous variability in atmospheric circulations and precipitation (Feng et al., 2013; Kataoka et al., 2014). Moreover, SSH anomalies along the west coast of Australia propagate to the west into the interior of the basin and modulates basin-wide meridional transport of the subtropical gyre in the south Indian Ocean (Eabry et al., 2021; Menezes & Vianna, 2019; Nagura & McPhaden, 2021; Volkov et al., 2020; Zhuang et al., 2013).

Previous studies pointed out that El Niño Southern Oscillation (ENSO) in the tropical Pacific Ocean is the primary forcing of SSH variability along the west coast of Australia. Surface wind anomalies in the tropical Pacific Ocean during ENSO events force SSH variations, which propagate from the tropical western Pacific Ocean to the region along the west coast of Australia via Indonesia archipelago (Clarke, 1991; Clarke & Liu, 1994; Feng et al., 2010, 2011; Potemra, 2001; Wijffels & Meyers, 2004). Local meridional winds can at times play a role, like during Ningaloo Niño events (Feng et al., 2013), but SSH along the west coast of Australia is more highly correlated with remote zonal winds in the equatorial Pacific Ocean on interannual timescales (Nagura & McPhaden, 2021).

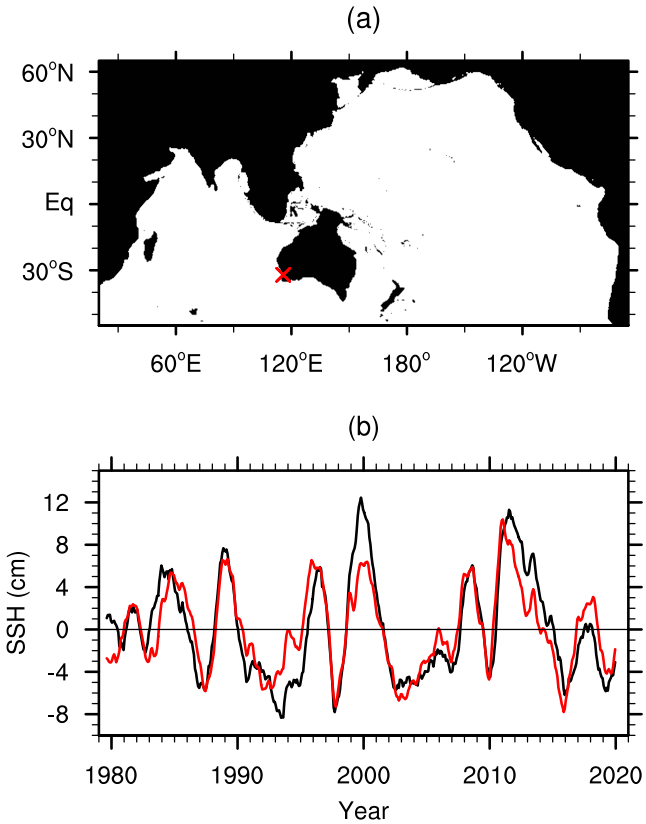

Figure 1. (a) Model domain. Black shades denote land grids. Note that ocean areas shallower than 200 m were designated as land and the marginal seas were filled by land. The red "X" indicates the tide gauge station at Fremantle. (b) Sea surface height (SSH) anomalies at Fremantle observed by tide gauge (black) and simulated by the 1.5-layer model in the control run (red). Both time series are detrended and smoothed by a 13-month running mean filter.

Using an ocean-atmosphere coupled general circulation model (CGCM), Hendon and Wang (2010) successfully predicted SSH anomalies at Fremantle with the lead times of 9 months, and Doi et al. (2013) predicted sea surface temperature (SST) anomalies off the northwest coast of Australia with a lead time of 6 months. The skill of these predictions in each case was attributed to the predictability of ENSO. However, the horizontal resolution of the ocean models was coarse (zonal grid intervals of 2°), which may have impeded the accurate simulation of SSH anomalies propagating through the Indonesia Archipelago and along the Australian coast. To mitigate this problem, Hendon and Wang (2010) adopted an empirical downscaling based on forecasts by a CGCM.

In this study we develop a much simpler methodology for predicting SSH anomalies along the west coast of Australia using a 1.5-layer dynamical model and ENSO-related winds. We illustrate the method by running the model in hindcast mode that is, "predicting" past variability assuming perfect knowledge about ENSO conditions. A true forecast system to predict future variations would also require prediction of ENSO. Thus, our results indicate an upper limit on how predictable SSH is in the southeast Indian Ocean based on the simple dynamical model. Even so, we are able to hindcast SSH anomalies along the west coast of Australia at lead times of up to 13 months, which significantly outperforms forecasts based on persisting anomalies forward in time from a given initial condition (i.e., a persistence forecast).

The result of this paper is structured as follows. Section 2 introduces data used and the model formulation. Section 3 describes the method of SSH hindcasts. Section 4 presents results, and Section 5 summarizes our main findings.

2. Data and Model

We obtained monthly averages of SSH from tide gauge observations at Fremantle (32°S, 116°E) along the west coast of Australia (red cross in Figure 1a). The time series at Fremantle is available since 1897. Data gaps shorter than 12 months were filled by linear interpolation. The inverted barometer effect was removed using sea level pressure obtained from ERA5 (Hersbach et al., 2020) for the period from 1979 to 2020 following the method of Ponte (2006). We used the multivariate ENSO index Version 2 (Wolter & Timlin, 1993) to define ENSO events. The multivariate ENSO index was computed by applying empirical orthogonal function analysis to anomalies of five variables in the tropical Pacific Ocean, that is, SST, sea level pressure and surface zonal and meridional winds obtained from JRA-55 reanalysis (Kobayashi et al., 2015) and outgoing longwave radiation obtained from the NOAA Climate Data Record. We also used monthly averages of surface wind stresses for the period from 1979 to 2020 provided by ERA5, which assimilates various satellite observations, including atmospheric motion vectors and scatterometer wind (Hersbach et al., 2020). Anomalies of tide gauge observations and ERA5 wind stresses were computed as the deviation from their monthly climatologies for the period from 1979 to 2020.

Nagura and Masumoto (2015) described the governing equations for the 1.5-layer model in detail. We used a linear version, with advection terms ignored. The model domain was prescribed to be 20°E–65°W and 55°S–65°N (Figure 1a) with a mean layer thickness and reduced gravity set to 150 and 0.05 m s^{-2}, respectively. The model has a horizontal model grid spacing of 0.5° in longitude and latitude and includes passages through the Indonesian Archipelago so to allow for simulation of the Indonesian Throughflow. The coastlines were obtained from ETOPO5 (ETOPO5, 1988). We averaged ETOPO5 over 0.5° × 0.5° boxes and

set grid points where the ocean bottom is shallower than 200 m as land. Some of the marginal seas were filled by land as is seen in Figure 1a. The model domain is blocked by walls at the western and southern boundaries. The layer thickness was restored toward the mean layer thickness near the southern wall with a restoring time scale of 10 days to prevent coastal Kelvin waves from propagating along this artificial boundary. A weak Newtonian damping (with the coefficient of 2×10^{-8} s^{-1}) and horizontal diffusivity (with the coefficient of 400 m^2 s^{-1}) were applied to momentum.

We forced the 1.5-layer model by ERA5 surface wind stress anomalies from 1979 to 2020, which we refer to as the control run. Simulated SSH anomalies compare well with tide gauge observations at Fremantle (Figure 1b), indicating that the model correctly reproduces processes by which SSH anomalies propagate from the western Pacific Ocean to the west coast of Australia. The correlation coefficient and neutral regression between the observed and simulated time series are respectively 0.87, which exceeds the 99% level of confidence, and 0.82 ± 0.22 (95% level of confidence), which is indistinguishable from unity.

3. Method

The target of our hindcasts is SSH anomalies at Fremantle, where a long record of tide gauge observations exists. Satellite altimetry shows that SSH anomalies are in phase along the west coast of Australia with the amplitude gradually decreasing poleward (Menezes & Vianna, 2019), which is a consequence of poleward propagation of coastal Kelvin waves. This indicates that SSH anomalies at Fremantle are representative of SSH variability all along the coast.

We conducted hindcast experiments using the 1.5-layer model in which the model was driven by ENSO-related winds obtained from regression analysis. Considering that ENSO events peak in boreal winter, we used the December–February (DJF) mean of the multivariate ENSO index as the index for ENSO events and regressed ERA5 surface wind stresses in each calendar month onto this index. The ENSO index was normalized by its standard deviation before the analysis. Considering the asymmetry of patterns of surface wind anomalies during El Niño and La Niña events (Hoerling et al., 1997; McPhaden & Zhang, 2009; Okumura & Deser, 2010), we conducted regression analysis separately for years when the DJF mean of the ENSO index was positive and for those when the index was negative. Regressed zonal wind stress anomalies are eastward east of 170°E in the tropical Pacific Ocean near the equator in DJF of El Niño years (Figure 2a), which turn westward in the subsequent June (Figure 2c). In DJF during a La Niña event, regressed zonal wind stress anomalies tend to be westward west of 150°W along the equatorial Pacific Ocean (Figure 2b) and last for about three years afterward (Figure 2d). In both of El Niño and La Niña events, regressed zonal wind stress anomalies in the tropical Pacific Ocean are slightly shifted to the south of the equator in DJF, which is consistent with results of Harrison (1987) and Okumura and Deser (2010). Note that the DJF mean of the multivariate ENSO index is highly correlated with SST anomalies in the equatorial Pacific Ocean between 160°W and 110°W (figure not shown) and representative of both the eastern Pacific and central Pacific ENSO events (Ashok et al., 2007; Kao & Yu, 2009; Kug et al., 2009; Larkin & Harrison, 2005). Marshall et al. (2015) argued that these two flavors of ENSO events have different impacts on sea level pressure and SST anomalies in the southeastern Indian Ocean. Owing to the short analysis period however, we do not distinguish between these two types of events in this study.

The ocean dynamical model was driven by a statistical model for wind stress anomalies during 12 ENSO events in which wind stresses were determined based on regression against the ENSO index as $\vec{\tau} = \vec{\alpha}(n)E(i)$, where $\vec{\tau}$ denotes the wind stress vector, $\vec{\alpha}$ regression coefficients for zonal and meridional wind stress, E the ENSO index, n lead months and i the index to ENSO events. ENSO events are defined as the years when the magnitude of the ENSO index exceeds its standard deviation (Figure 2e). The hindcast experiments were initialized from four start dates: June in Year 0, September in Year 0, December in Year 0 or March in Year 1 (abbreviated as June[0], September[0], December[0], and March[1] hereafter). Here, Year 0 means the year when an ENSO event develops and grows to its peak (e.g., 1982 for 1982–1983 El Niño event) and Year 1 means the year subsequent to Year 0. The hindcast experiments were integrated for 3–4 years, to December of Year 4. Output from the control run were used as the initial conditions. Predicted SSH anomalies at Fremantle are smoothed by a 13-month running mean filter and compared with similarly smoothed SSH anomalies obtained from tide gauge.

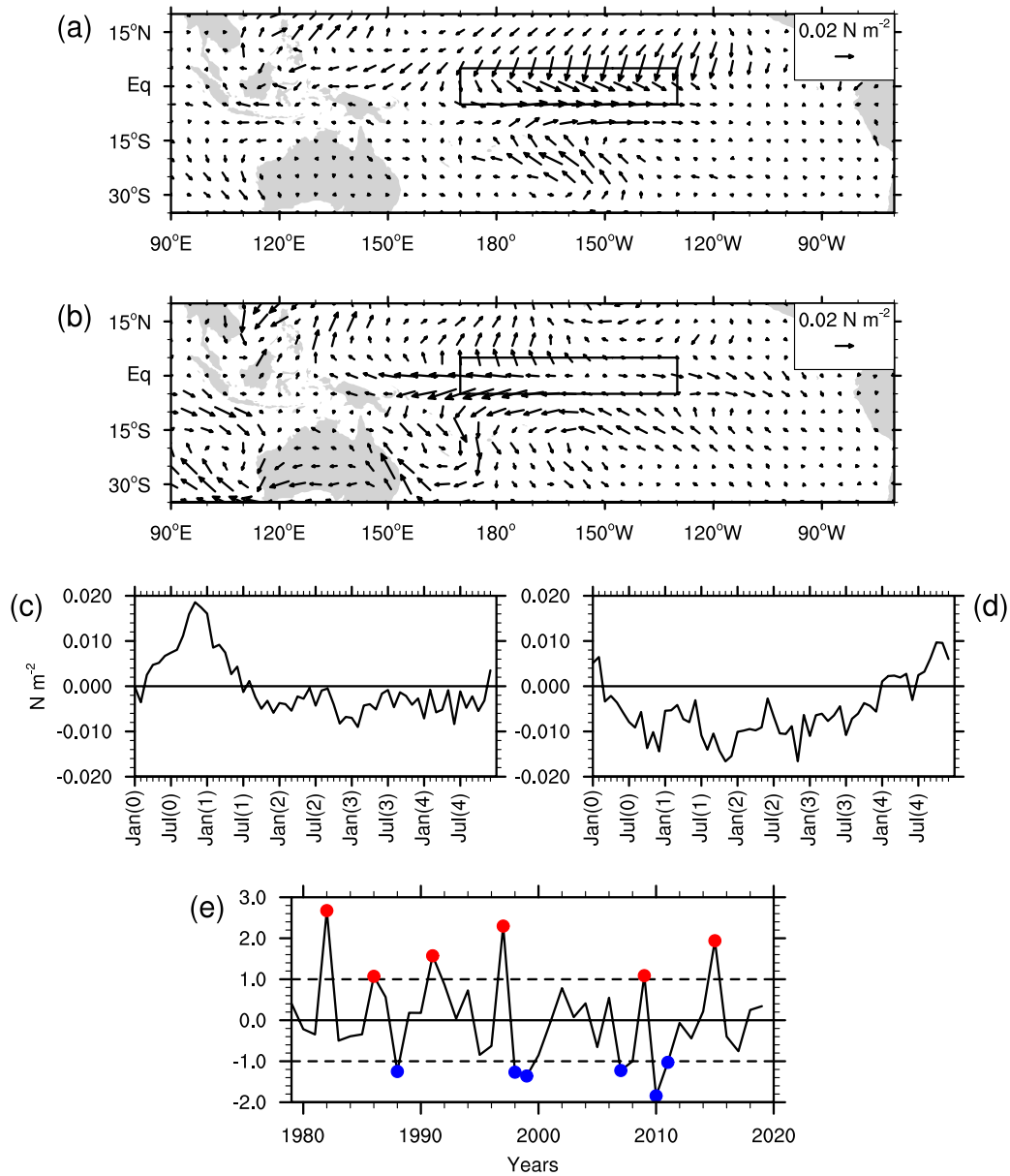

Figure 2. (a) December–February (DJF) mean of surface wind stress anomalies regressed onto the DJF mean of the multivariate El Niño Southern Oscillation (ENSO) index for El Niño events. The DJF mean of the ENSO index was normalized by its standard deviation before regression analysis. Box indicates the region from 5°S to 5°N and from 170°E to 130°W. (b) As in (a), but for La Niña events. (c) Time series of zonal wind stress anomalies regressed onto the DJF mean of the multivariate ENSO index for El Niño events averaged over the box shown in (a). (d) As in (c), but for La Niña events. (e) DJF mean of the multivariate ENSO index. The index is normalized by its standard deviation. The value at 1980 shows the average over December 1980 to February 1981, for example. Dashed lines show ±1. Red and blue filled circles illustrate El Niño and La Niña years, respectively.

We also tested a purely statistical forecast approach by regressing observed Fremantle SSH anomalies onto the DJF mean of the ENSO index separately for El Niño and La Niña events. A statistical hindcast was made as $h = \beta(n)E(i)$, where h denotes Fremantle SSH anomalies and β is the regression coefficients of Fremantle SSH. We compare results for this model with the dynamically based prediction scheme in the next section.

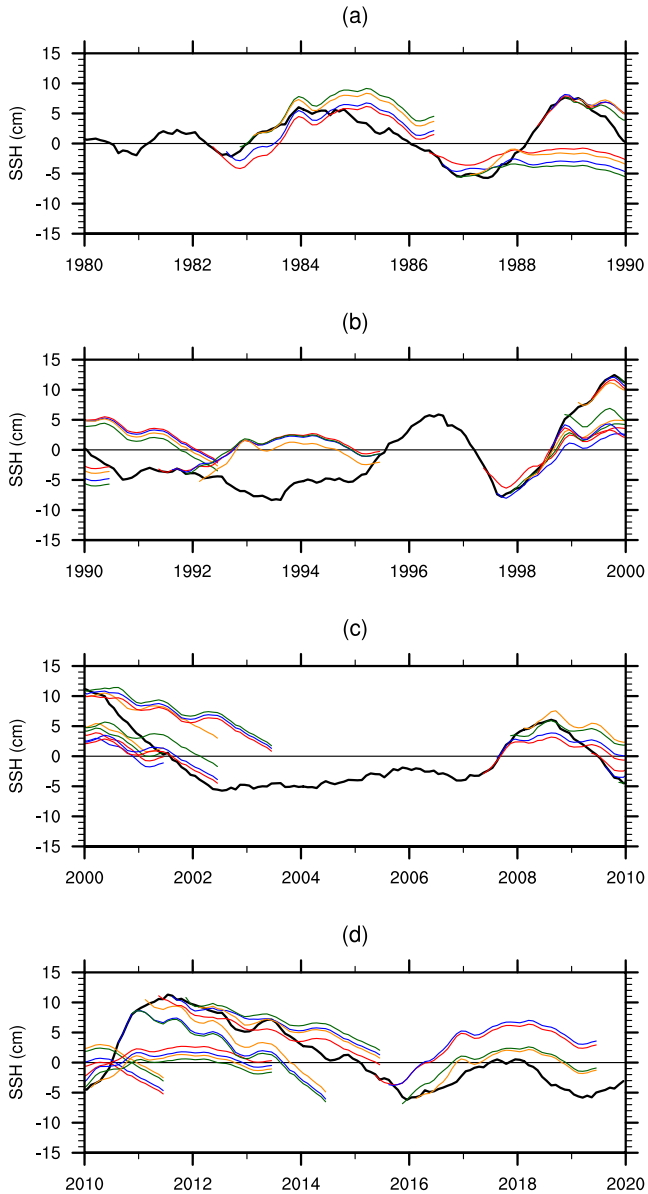

Figure 3. Sea surface height (SSH) anomalies at Fremantle observed by tide gauge (black) and hindcasted by the 1.5-layer model and the statistical model for El Niño Southern Oscillation (ENSO)-related winds (red, blue, green, and orange lines) for the period (a) from 1980 to 1990, (b) from 1990 to 2000, (c) from 2000 to 2010 and (d) from 2010 to 2020. A 13-month running mean was applied. Observed time series was detrended. Red, blue, green, and orange lines show results for which the hindcast experiment starts since June in Year 0, September in Year 0, December in Year 0 and March in Year 1, respectively.

4. Results

Hindcasted SSH anomalies compare well with observed anomalies in 1982–1986, 1997–2002, 2007–2011, 2011–2014, and 2015–2019 (Figure 3). Model hindcasts are less successful during the period 1986–1995. In 1986–1987, warm SST anomalies persisted for a few years in the equatorial Pacific Ocean and the 1991–1992 event was the start of 4 successive warm years (Figure 2e). These events did not follow the evolution of El Niño events obtained from our regression analysis, in which El Niño peaks in December and turns to La Niña in next boreal summer (Figure 2c), as is observed in 1982–1983, 1997–1998, and 2015–2016. However, except in these two events, model hindcasts were relatively skillful.

We compare results between model hindcasts and persistence in terms of anomaly correlation coefficients and root-mean-square (RMS) differences (Figure 4). Persistence forecasts assume that SSH anomalies at the initial time remain constant afterward. Correlation coefficients and RMS differences were computed in comparison with tide gauge observations at Fremantle. At most of the lead times, correlation coefficients are higher and RMS differences are lower for model hindcasts than for persistence forecasts, which indicates that model hindcasts outperform persistence forecasts.

For model hindcasts, the anomaly correlation drops below the 99% confidence level at lead times of 10–13 months. The decrease of correlation does not clearly depend on the season when the hindcast starts. On the other hand, correlation drops below the 99% level at a lead time of 5 months for persistence forecasts that start from June(0), whereas correlation becomes lower than the 99% level at lead times of 10, 9, and 8 months for persistence forecasts that start from September(0), December(0), and March(1), respectively. This seasonality in skill may reflect the fact that ENSO events are still developing in June(0) and related SSH anomalies at Fremantle tend to be small in amplitude and susceptible to noise contamination, which makes a persistence forecast less reliable. On the other hand, ENSO-related anomalies have grown in amplitude by September and December and begin to decay in amplitude in March in Year 1. A persistence forecast is relatively more reliable from these start dates. As a consequence, the difference in skill between model hindcasts and persistence forecasts is largest for simulations that start from June(0).

RMS differences are consistent with the above considerations. RMS differences for model hindcasts exceed the standard deviation of observed Fremantle SSH anomalies first at lead times of 9–13 months. Those for persistence forecasts become larger than the standard deviation first at lead times of 4, 6, 8, and 6 months, if the forecast starts from June(0), September(0), December(0), and March(1), respectively. Again, the difference in skill between model hindcasts and persistence forecasts is largest when the forecasts start from June(0).

The lead time of model hindcasts that start from June(0) is 13 months, based on when the correlation between observations and hindcast results drops below the 99% confidence level. This lead time is partly due to the statistical model for ENSO-related winds. Zonal wind anomalies during an El Niño event decay in boreal spring in Year 1 (Figure 2c), which provides 9 months lead time if a hindcast starts from June(0).

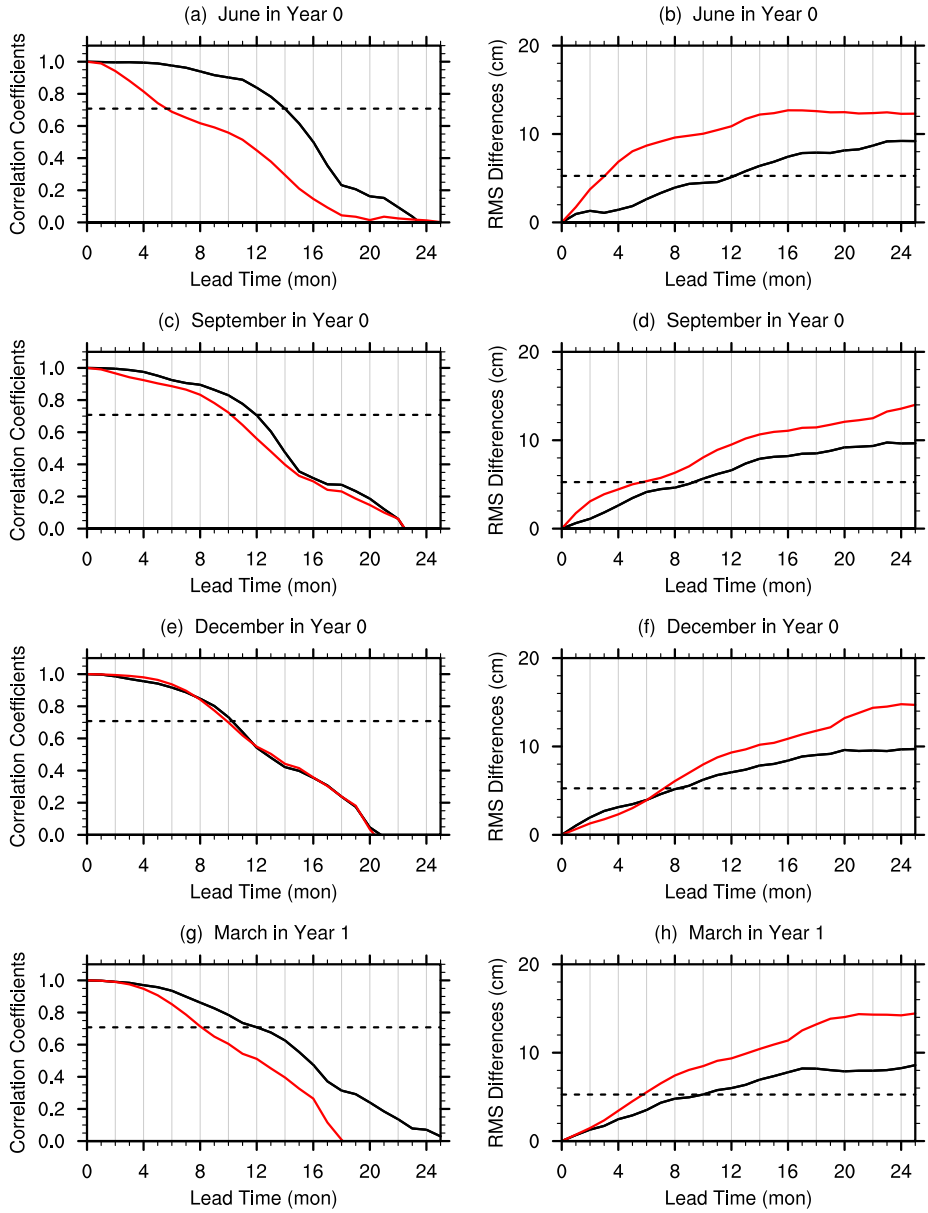

Figure 4. (a, c, e, g) Anomaly correlation coefficients and (b, d, f, h) root-mean-square (RMS) differences between tide gauge observations and numerical model hindcasts (black line) and between tide gauge observations and persistence forecasts (red line) at Fremantle. Dashed line shows the 99% confidence limit in (a, c, e, g) and the standard deviation of observed Fremantle sea surface height (SSH) anomalies in (b, d, f, h). The hindcast experiments start in (a and b) June in Year 0, (c and d) September in Year 0, (e and f) December in Year 0 and (g and h) March in Year 1. Correlations and RMS differences were computed using the time series smoothed by a 13-month running mean.

It is likely that the response time of SSH variability along the west coast of Australia to zonal winds in the equatorial Pacific is involved as well. Nagura and McPhaden (2021) showed that the time lag between zonal wind anomalies in the equatorial Pacific Ocean and SSH anomalies along the west coast of Australia is about 5 months, which is owing to the time required for Pacific winds to force local SSH variability plus the time required for SSH variability to propagate to the west coast of Australia via the Indonesia Archipelago. The sum ($9 + 5 = 14$ months) roughly explains the lead time of the model hindcasts.

Hindcast skill discussed above was evaluated using time series smoothed by a 13-month running mean filter. The skill evaluated from unsmoothed time series was noisy, but still correlation for model hindcasts

starting from June(0) exceeds the 99% confidence level up to a lead time of 11 months (Figures S1 and S2). Correlation for persistence forecasts starting from June(0) drops below the 99% level at a lead time of 3 months, which again indicates that the model outperforms persistence.

For comparison with our dynamical model results, we compared the purely statistical model hindcasts of Fremantle SSH anomalies using the multivariate ENSO index as a predictor (Figure S3). Results from the purely statistical model show correlations higher than the 99% confidence level at lead times up to 14 months from June(0) initial conditions (Figure S3a), which is comparable to the correlation skill of the numerical model hindcasts (Figure 4a). On the other hand, RMS differences for the purely statistical hindcasts starting from June(0) are as large as those for persistence (Figure S3b) and larger than those for the numerical model hindcasts (Figure 4b). Similarly, anomaly correlations for the purely statistical hindcasts starting from September(0) and December(0; Figures S3c and S3e) are comparable with those for the numerical model hindcasts (Figures 4c and 4e), but RMS differences for the statistical hindcasts are larger than those for numerical model hindcasts (Figures 4d, 4f, S3d and S3f). For hindcasts starting from March(1), correlations are lower and RMS differences are larger for the statistical model than for the numerical model (Figures 4g, 4h, S3g and S3h). Thus, the purely statistical model is able to simulate the phase of SSH anomalies as well as the numerical model, but it is worse than the numerical model in simulating anomaly amplitudes.

5. Summary

This study describes a statistical-dynamical forecast methodology for SSH anomalies along the west coast of Australia using a 1.5-layer ocean model and a statistical atmospheric model related to ENSO. The ocean model is linear with realistic Indo-Pacific Ocean coastlines, including passages through the Indonesian Archipelago. The atmospheric model was constructed by regressing ERA5 surface wind stress onto the DJF mean of the multivariate ENSO index. We illustrate the skill of this methodology by hindcasting past variability assuming perfect knowledge of ENSO. Results showed that model hindcasts outperform persistence in terms of anomaly correlation coefficients and RMS differences. The difference in skill between model hindcasts and persistence is largest when hindcasts start from June(0). An ENSO event is not mature yet in June(0) and a persistence forecast starting from this time is able to reasonably predict SSH anomalies only up to 5 months in advance, based on when the correlation between observations and forecasts drops below the 99% confidence level. On the other hand, model hindcasts starting from June(0) are able to simulate SSH anomalies at Fremantle up to 13 months in advance, which clearly outperforms persistence. If the hindcast starts from December, the difference in skill between model hindcasts and persistence is relatively small, because an ENSO event matures in December and SSH anomalies are large in amplitude, which makes persistence more reliable.

We also developed a purely statistical forecast model, which is formulated by regressing Fremantle SSH anomalies onto the multivariate ENSO index. The statistical model is able to simulate the phase of SSH anomalies, but its skill in simulating the amplitude of anomalies is worse than the numerical ocean model methodology. It is possible that a more sophisticated multi-predictor statistical model would exhibit improved performance, but our comparisons nonetheless emphasize the value of using a dynamically based ocean prediction scheme.

In summary, we have shown that SSH anomalies along the west coast of Australia can be predicted using a simple dynamical ocean model forced by ENSO-related winds in the equatorial Pacific. We have illustrated this by running the model in hindcast mode, using the DJF means of the multivariate ENSO index to compute surface wind forcing (Section 3). To make a realistic prediction from June, one would also need to predict the mean of the ENSO index for the coming DJF as is done in true prediction systems like those discussed in Hendon and Wang (2010) and Doi et al. (2013). While it is beyond the scope of this study to make actual forecasts, application of our methodology can be useful as a baseline for gauging the performance of forecasts made by more sophisticated CGCM systems.

Data Availability Statement

Tide gauge SSH data were obtained from the website of Permanent Service for Mean Sea Level (https://www.psmsl.org/data/obtaining/). The multivariate ENSO index Version 2 was obtained from the National Oceanic and Atmospheric Administration/the Physical Sciences Laboratory (https://psl.noaa.gov/enso/mei/).

Acknowledgments
The authors thank two anonymous reviewers and Chidong Zhang of NOAA/PMEL for their helpful comments. This work was supported by JSPS Grants-in-Aid for Scientific Research (KAKENHI) grant JP18K03750. PMEL contribution number 5260.

References

Ashok, K., Behera, S. K., Rao, S. A., Weng, H., & Yamagata, T. (2007). El Niño Modoki and its possible teleconnection. *Journal of Geophysical Research*, *112*, C11007. https://doi.org/10.1029/2006JC003798

Clarke, A. J. (1991). On the reflection and transmission of low-frequency energy at the irregular western Pacific Ocean boundary. *Journal of Geophysical Research*, *96*, 3289–3305. https://doi.org/10.1029/90jc00985

Clarke, A. J., & Liu, X. (1994). Interannual sea level in the northern and eastern Indian Ocean. *Journal of Physical Oceanography*, *24*(6), 1224–1235. https://doi.org/10.1175/1520-0485(1994)024<1224:ISLITN>2.0.CO;2

Doi, T., Behera, S. K., & Yamagata, T. (2013). Predictability of the Ningaloo Niño/Niña. *Scientific Reports*, *3*, 2892. https://doi.org/10.1038/srep02892

Eabry, M. D., Taschetto, A. S., Maharaj, A. M., & Sen Gupta, A. (2021). What determines the lagged ENSO response in the south-west Indian Ocean? *Geophysical Research Letters*, *48*. https://doi.org/10.1029/2020GL091958

ETOPO5. (1988). Digital relief of the surface of the earth. In *Worldwide Bathymetry/Topography Data Announcement* (Vol. 88). National Geophysical Data Center.

Feng, M., Böning, C., Biastoch, A., Behrens, E., Weller, E., & Masumoto, Y. (2011). The reversal of the multidecadal trends of the equatorial Pacific easterly winds, and the Indonesian Throughflow and Leeuwin Current transports. *Geophysical Research Letters*, *38*, L11604. https://doi.org/10.1029/2011GL047291

Feng, M., McPhaden, M. J., & Lee, T. (2010). Decadal variability of the Pacific subtropical cells and their influence on the southeast Indian Ocean. *Geophysical Research Letters*, *37*, L09606. https://doi.org/10.1029/2010GL042796

Feng, M., McPhaden, M. J., Xie, S.-P., & Hafner, J. (2013). La Niña forces unprecedented Leeuwin Current warming in 2011. *Scientific Reports*, *3*(1277), 3. https://doi.org/10.1038/srep01277

Harrison, D. E. (1987). Monthly mean island surface winds in the central tropical Pacific and El Niño events. *Monthly Weather Review*, *115*, 3133–3145. https://doi.org/10.1175/1520-0493(1987)115<3133:mmiswi>2.0.co;2

Hendon, H. H., & Wang, G. (2010). Seasonal prediction of the Leeuwin Current using the POAMA dynamical seasonal forecast model. *Climate Dynamics*, *34*, 1129–1137. https://doi.org/10.1007/s00382-009-0570-3

Hersbach, H., Bell, B., Berrisford, P., Hirahara, S., Horányi, A., Muñoz-Sabater, J., et al. (2020). The ERA5 global reanalysis. *Quarterly Journal of the Royal Meteorological Society*, *146*, 1999–2049. https://doi.org/10.1002/qj.3803

Hoerling, M. P., Kumar, A., & Zhong, M. (1997). El Niño, La Niña, and the nonlinearity of their teleconnections. *Journal of Climate*, *10*, 1769–1786. https://doi.org/10.1175/1520-0442(1997)010<1769:enolna>2.0.co;2

Kao, H.-Y., & Yu, J.-Y. (2009). Contrasting eastern-Pacific and central-Pacific types of ENSO. *Journal of Climate*, *22*, 615–632. https://doi.org/10.1175/2008JCLI2309.1

Kataoka, T., Tozuka, T., Behera, S., & Yamagata, T. (2014). On the Ningaloo Niño/Niña. *Climate Dynamics*, *43*, 1463–1482. https://doi.org/10.1007/s00382-013-1961-z

Kobayashi, S., Ota, Y., Harada, Y., Ebita, A., Moriya, M., Onoda, H., et al. (2015). The JRA-55 reanalysis: General specifications and basic characteristics. *Journal of the Meteorological Society of Japan. Ser II*, *93*(1), 5–48. https://doi.org/10.2151/jmsj.2015-001

Kug, J.-S., Jin, F.-F., & An, S.-I. (2009). Two types of El Niño events: Cold tongue El Niño and warm pool El Niño. *Journal of Climate*, *22*, 1499–1515. https://doi.org/10.1175/2008JCLI2624.1

Larkin, N. K., & Harrison, D. E. (2005). Global seasonal temperature and precipitation anomalies during El Niño autumn and winter. *Geophysical Research Letters*, *32*, L16705. https://doi.org/10.1029/2005GL022860

Marshall, A. G., Hendon, H. H., Feng, M., & Schiller, A. (2015). Initiation and amplification of the Ningaloo Niño. *Climate Dynamics*, *45*, 2367–2385. https://doi.org/10.1007/s00382-015-2477-5

McPhaden, M. J., & Zhang, X. (2009). Asymmetry in zonal phase propagation of ENSO sea surface temperature anomalies. *Geophysical Research Letters*, *36*, L13703. https://doi.org/10.1029/2009GL038774

Menezes, V. V., & Vianna, M. L. (2019). Quasi-biennial Rossby and Kelvin waves in the South Indian Ocean: Tropical and subtropical modes and the Indian Ocean dipole. *Deep-Sea Research II*, *166*, 43–63. https://doi.org/10.1016/j.dsr2.2019.05.002

Nagura, M., & Masumoto, Y. (2015). A wake due to the Maldives in the eastward Wyrtki jet. *Journal of Physical Oceanography*, *45*, 1858–1876. https://doi.org/10.1175/jpo-d-14-0191.1

Nagura, M., & McPhaden, M. J. (2021). Interannual variability in sea surface height at southern mid-latitudes of the Indian Ocean. *Journal of Physical Oceanography*, *51*, 1595–1609. https://doi.org/10.1175/jpo-d-20-0279.1

Okumura, Y., & Deser, C. (2010). Asymmetry in the duration of El Niño and La Niña. *Journal of Climate*, *23*, 5826–5843. https://doi.org/10.1175/2010jcli3592.1

Ponte, R. M. (2006). Low-frequency sea level variability and the inverted barometer effect. *Journal of Atmospheric and Oceanic Technology*, *23*, 619–629. https://doi.org/10.1175/jtech1864.1

Potemra, J. T. (2001). Contribution of equatorial Pacific winds to southern tropical Indian Ocean Rossby waves. *Journal of Geophysical Research*, *106*(C2), 2407–2422. https://doi.org/10.1029/1999JC000031

Volkov, D. L., Lee, S.-K., Gordon, A. L., & Rudko, M. (2020). Unprecedented reduction and quick recovery of the South Indian Ocean heat content and sea level in 2014-2018. *Sciences Advances*, *6*, eabc1151. https://doi.org/10.1126/sciadv.abc1151

Wijffels, S., & Meyers, G. (2004). An intersection of oceanic waveguides: Variability in the Indonesian throughflow region. *Journal of Physical Oceanography*, *34*(5), 1232–1253. https://doi.org/10.1175/1520-0485(2004)034<1232:AIOOWV>2.0.CO;2

Wolter, K., & Timlin, M. S. (1993). Monitoring ENSO in COADS with a seasonally adjusted principal component index. In Proceedings of the 17th Climate Diagnostics Workshop, Norman, OK, NOAA/NMC/CAC, NSSL, Oklahoma Climate Survey, CIMMS and the School of Meteorology, (pp. 52–57). University of Oklahoma.

Zhuang, W., Feng, M., DuSchiller, Y. A., Wang, D., & Wang, D. (2013). Low-frequency sea level variability in the southern Indian Ocean and its impacts on the oceanic meridional transports. *Journal of Geophysical Research: Oceans*, *118*, 1302–1315. https://doi.org/10.1002/jgrc.20129